WILEY-VCH

Understanding the Early Stages of Nickel Sulfide Nanocluster Growth: Isolation of Ni_3, Ni_4, Ni_5, and Ni_8 Intermediates

*Alexander J. Touchton, Guang Wu, Trevor W. Hayton**

*Department of Chemistry & Biochemistry, University of California, Santa Barbara, California 93106, United States

E-mail: hayton@chem.ucsb.edu

Keywords: nickel, thiolate, sulfide, nanocluster, synthesis, mechanism

Abstract: Addition of sub-stoichiometric quantities of PEt_3 and PhSSPh to a solution of $[Ni(1,5\text{-cod})_2]$ generates a mixture of $[Ni_3(SPh)_4(PEt_3)_3]$ (**1**), unreacted $[Ni(1,5\text{-cod})_2]$, and $[(1,5\text{-cod})Ni(PEt_3)_2]$, according to ^1H and $^{31}P\{^1H\}$ NMR spectroscopic monitoring of the *in situ* reaction mixture. On standing, complex **1** converts into $[Ni_4(S)(Ph)(SPh)_3(PEt_3)_3]$ (**2**), via formal addition of a "Ni(0)" equivalent, coupled with a C–S oxidative addition step, which simultaneously generates the Ni-bound phenyl ligand and the μ_3-sulfide ligand. Upon gentle heating, complex **2** converts into a mixture of $[Ni_5(S)_2(SPh)_2(PEt_3)_5]$ (**3**) and $[Ni_8(S)_5(PEt_3)_7]$ (**4**), via further addition of "Ni(0)" equivalents, in combination with a series of C–S oxidative addition and C–C reductive elimination steps, which serve to convert thiophenolate ligands into sulfide ligands and biphenyl. The presence of **1**-**4** in the reaction mixture was confirmed by their independent syntheses and subsequent spectroscopic characterization. Overall, this work provides an unprecedented level of detail of the early stages of Ni nanocluster growth, and highlights the fundamental reaction steps (i.e., metal atom addition, C–S oxidative addition, and C–C reductive elimination) that are required to grow an individual cluster. In addition, our results highlight the challenges inherent in the synthesis of low-valent thiolate-stabilized Ni nanoclusters, whose isolation will require the suppression of C–S bond oxidative addition.

1. Introduction

The last 10 years have seen significant progress in the synthesis of thiolate-stabilized group 11 nanoclusters (NCs).[1-6] These advancements have been driven, in part, by the deployment of the single phase Brust-Schiffrin synthetic protocol, which has allowed for the rapid diversification of coinage metal NCs,[4] such as $[Au_{102}(p\text{-MBA})_{44}]$ (*p*-MBA = *para*-mercaptobenzoic acid),[7] $[Ag_{25}(S\text{-}2,4\text{-}Me_2C_6H_3)_{18}]^-$,[8] and $[Cu_{61}(S)_6(S^tBu)_{26}Cl_6H_{14}]^+$.[9] In a typical synthesis, small $[M(SR)]_n$ oligomers are generated in the early stages of the reaction by combining a metal halide precursor with excess HSR. These oligomers are then reduced by $NaBH_4$ to generate low-valent $[M_x(SR)_y]$-type ($x > y$) clusters, which feature at least some M(0) character.[10-11] In contrast, when this synthetic strategy is applied to other transition metals, such as Co and Ni, only the products of salt metathesis, i.e., small M(II) thiolate clusters, are isolated[6, 12-14] — the metal reduction step is not observed. This result is not entirely surprising, given that it is much harder to reduce Co^{2+} and Ni^{2+} than it is to reduce the group 11 M^+ cations.[15] Access to these materials is of interest because Co- and Ni-thiolate nanoclusters are anticipated to be paramagnetic, unlike group 11 nanoclusters, which are typically diamagnetic. Thus, they and could be useful for a variety of magnetism applications, including ferrofluids and quantum computing.[16-18] Additionally, their properties can be easily tuned by changing the thiolate substituent, in contrast to previously reported sulfide-capped nanoclusters.[19-20]

In an effort to solve the metal reduction problem, several groups have employed the use of M(0)-containing starting materials, instead of the traditional M(II) salts.[21-23] For example, we recently used $[Ni^{II}(\eta^3\text{-}CPh_3)_2]$ as a source of Ni(0) to generate the low-valent phosphinidene cluster, $[Ni_3(PPh)(PPh_2)_2(PPh_3)_3]$.[24] Similarly, Roy and co-workers recently employed commercially available Ni(0) synthon, $[Ni(1,5\text{-cod})_2]$, to generate a series of low-valent Ni phosphinidene clusters.[25] Steigerwald and co-workers have also employed $[Ni(1,5\text{-cod})_2]$ as a source of Ni(0) to access low-valent, chalcogenide-capped Ni nanoclusters.[26-28]

In this work, we sought to evaluate whether $[Ni(1,5\text{-cod})_2]$ could be used to access low-valent $[Ni_x(SR)_y]$-type ($x > y$) clusters, a class of materials which remains unknown despite several attempts at their isolation.[6, 13-14] To access these materials we envisioned that addition of sub-stoichiometric quantities of diphenyl disulfide (PhSSPh), which can act as a thiolate source upon S–S bond cleavage, to $[Ni(1,5\text{-cod})_2]$, in the presence of a phosphine capping ligand, would generate the desired low-valent, thiolate-protected Ni nanoclusters.

Herein, we report the conversion of [Ni(1,5-cod)$_2$] into the low-valent Ni thiolate cluster, [Ni$_3$(SPh)$_4$(PEt$_3$)$_3$] (**1**), which subsequently converts into a mixture of the low-valent Ni sulfide-containing nanoclusters, [Ni$_5$(S)$_2$(SPh)$_2$(PEt$_3$)$_5$] (**3**) and [Ni$_8$(S)$_5$(PEt$_3$)$_7$] (**4**), via a series of Ni(0) addition, C–S oxidative addition, and C–C reductive elimination steps. In addition, the isolation of the organometallic phenyl-containing Ni$_4$ intermediate, [Ni$_4$(S)(Ph)(SPh)$_3$(PEt$_3$)$_3$] (**2**), from the reaction mixture conclusively demonstrates that the sulfide ligands in **3** and **4** form via C–S oxidative addition. The isolation of these intermediates provides an unprecedented level of detail of Ni sulfide nanocluster growth, which may enable the targeted synthesis of larger Ni sulfide clusters.

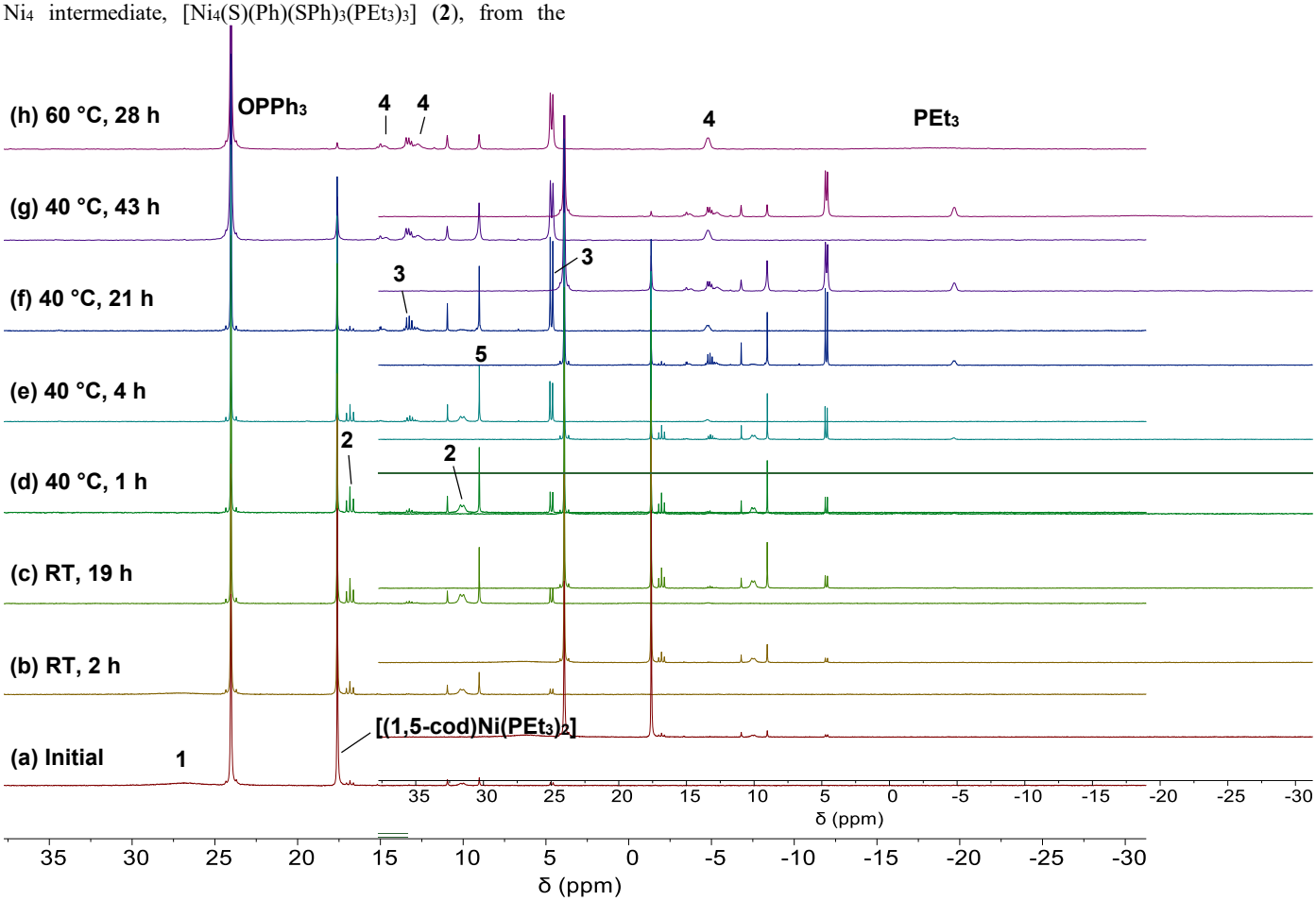

Figure 1. ^{31}P{^{1}H} NMR spectroscopic monitoring the reaction of [Ni(1,5-cod)$_2$] (8 equiv) with PEt$_3$ (7 equiv) and PhSSPh (2.5 equiv) in toluene-*d*$_8$ with Ph$_3$PO added as internal standard.

2. Results and Discussion

2.1. ^{31}P NMR Spectroscopic Monitoring of the Reaction of [Ni(1,5-cod)$_2$] with PEt$_3$ and PhSSPh

Addition of 7 equiv of PEt$_3$ and 2.5 equiv of diphenyl disulfide to a suspension of 8 equiv of [Ni(1,5-cod)$_2$] in toluene-*d*$_8$, results in an immediate color change to dark brown.[29] The ^{31}P{^{1}H} NMR spectrum of this mixture features a sharp resonance at 17.6 ppm assignable to [(1,5-cod)Ni(PEt$_3$)$_2$] (Scheme 1, Figure 1a, Table S2),[30] as well as a broad resonance at 27 ppm, which we have assigned to the trimetallic thiolate cluster, [Ni$_3$(SPh)$_4$(PEt$_3$)$_3$] (**1**). Also present in this spectrum are minor resonances at 16.8 (t, J_{PP} = 33.8 Hz) and 10.1 (br d, J_{PP} = 28.4 Hz), which we have assigned to the sulfide-containing Ni$_4$ cluster, [Ni$_4$(S)(Ph)(SPh)$_3$(PEt$_3$)$_3$] (**2**). These resonances are present in a 1:2 ratio, respectively. This spectrum also features a minor peak at 9.0 ppm, which we have tentatively assigned to the square planar Ni(II) phenyl complex, [Ni(Ph)(SPh)(PEt$_3$)$_2$] (**5**) (see below for more discussion).

Upon standing for 2 h at room temperature, the broad resonance assignable to **1** decreases in intensity, while the resonances assignable to **2** and **5** grow in intensity (Figure 1b, Table S2). On standing overnight at room temperature, the resonance assignable to **1** disappears, the resonance assignable to [(1,5-cod)Ni(PEt$_3$)$_2$] decreases in intensity, while resonances assignable to **2** and **5** continue to grow in intensity (Figure 1c). This spectrum also features minor resonances at 4.7 ppm and 13.4 ppm, which appear in a 1:5 ratio and are assignable to the sulfide thiolate cluster, [Ni$_5$(S)$_2$(SPh)$_2$(PEt$_3$)$_5$] (**3**). After heating the sample to 40 °C for 1 h, the resonances assignable to **2** decrease in relative intensity, while those assignable to **3** increase in intensity (Figure 1d). Further heating the sample at 40 °C for a total of 43 h results in a disappearance of the resonances assignable to **2**, while those assignable to **3** increase in intensity (Figure 1g). Also present in this spectrum are broad resonances at –4.8 ppm, 12.8 ppm, and 14.6 ppm. These resonances appear in a 4:2:1 ratio and are assignable to the Ni$_8$ sulfide nanocluster, [Ni$_8$(S)$_5$(PEt$_3$)$_7$] (**4**). Finally, further heating of the solution to 60 °C for 28 h results in the decrease of resonances assignable to **3** and **5**, while those assignable to **4** continue to increase in intensity (Figure 1h). Overall, these

data are consistent with a reaction sequence in which complex **1** is generated initially, but then converts into **2**, which then converts into **3** and then **4** upon heating. The *in situ* ^{1}H NMR spectra and ESI-MS data of the reaction mixture are broadly consistent with the speciation data revealed by our ^{31}P{^{1}H} NMR spectra (Figure 1). These data are discussed in further detail in the Supporting Information. Additionally, the *in situ* ^{1}H NMR spectra reveal the formation of biphenyl as a major by-product of the reaction (see below for more discussion of this observation).

2.2. Independent Synthesis and Characterization of Complexes 1, 2, 3, and 4

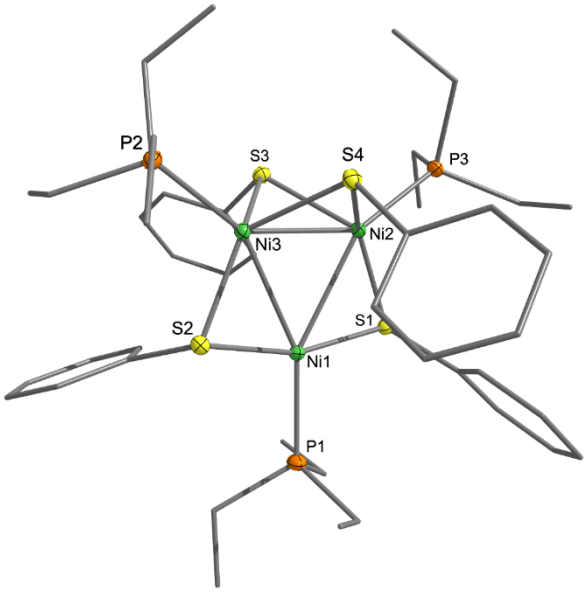

Figure 2. ORTEP diagram of **1** with thermal ellipsoids plotted at 50%. All hydrogen atoms omitted for clarity. Carbon atoms shown as wireframe. Selected bond lengths (Å): Ni1–Ni2 = 2.6481(6), Ni1–Ni3 = 2.6699(6), Ni2–Ni3 = 2.5100(6).

To confirm the formulation of complex **1**, we endeavored to independently prepare and isolate this species. In this regard, complex **1** could be successfully prepared by addition of 2 equiv of PhSSPh to a suspension of [Ni(1,5-cod)$_2$] (3 equiv) and PEt$_3$ (3 equiv) in cold diethyl ether (–25 °C). Work-up of the reaction mixture furnished [Ni$_3$(SPh)$_4$(PEt$_3$)$_3$] (**1**), which could be isolated in 62% yield as a deep brown crystalline solid (Scheme 1). Its room temperature ^{31}P{^{1}H} NMR spectrum in toluene-*d*$_8$ features a broad singlet at 32 ppm, consistent with the results from the *in situ* spectroscopic monitoring study (Figure S5, Figure 1). On cooling the NMR sample to –79 °C, however, this resonance decoalesces into two peaks at 2 ppm and –7 ppm, which are assignable to two magnetically inequivalent PEt$_3$ environments in a 2:1 ratio (Figure S8), consistent with the solid-state molecular structure (see below). Its room temperature ^{1}H NMR spectrum in benzene-*d*$_6$ also supports its presence in the *in situ* spectroscopic monitoring experiment (Figures S2-S4). The ESI-MS of **1** in THF, acquired in positive ion mode, further supports the proposed formulation. Specifically, peaks at 966.21 *m/z* and 857.19 m/z are ascribable to [M]$^+$ (calcd 966.12 m/z) and [M – SPh]$^+$ (calcd 857.11 *m/z)*, respectively (Figures S23–S26).

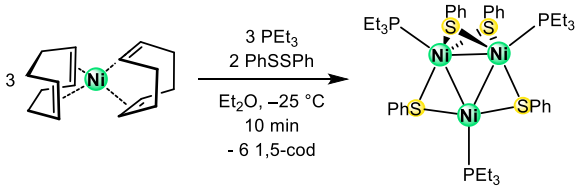

Scheme 1. Synthesis of **1**.

Complex **1** crystallizes in the monoclinic space group P2$_1$/*n*, and its solid-state molecular structure is shown in Figure 2. It features a triangular arrangement of nickel atoms with two unique thiophenolate environments and two unique PEt$_3$ environments, consistent with its low temperature ^{31}P{^{1}H} NMR spectrum. The Ni–Ni bond lengths are 2.5100(6), 2.6699(6), and 2.6481(6) Å, which are consistent with those expected for Ni–Ni single bonds (formal shortness ratio (FSR) = 1.01, 1.07, and 1.06, respectively).[31-32] For further comparison, the Ni–Ni distances in the Ni(II) thiolate cluster, [Ni(SCH$_2$CH$_2$Ph)$_2$]$_6$, are much longer (2.84–2.94 Å).[13] Complex **1** features an average oxidation state of +1.33, but given the Ni–Ni bonding and the observed diamagnetism, the Ni valence electrons in **1** must be delocalized over all three Ni centers.

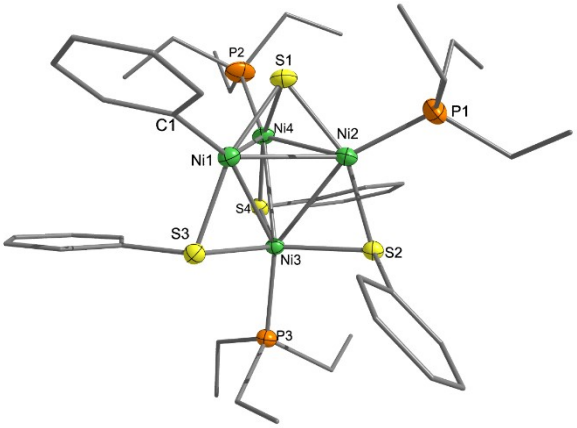

Figure 3. ORTEP diagram of **2**·0.5C$_6$H$_{14}$ with thermal ellipsoids plotted at 50%. Hydrogen atoms and hexane solvate molecule omitted for clarity. Carbon atoms shown as wireframe. Only one set of ethyl groups are displayed for the disordered ethyl groups of P1 and P2. Selected bond lengths (Å): Ni1–Ni4 = 2.5312(8), Ni2–Ni4 = 2.5572(9), Ni1–Ni2 = 2.5640(8), Ni3–Ni4 = 2.6494(8), Ni2–Ni3 = 2.6853(9), Ni1–Ni3 = 2.7021(7).

We also attempted to independently generate complex **2**. This species could be specifically targeted by reaction of 4 equiv of [Ni(1,5-cod)$_2$] with 3 equiv of PEt$_3$ and 2 equiv of PhSSPh in Et$_2$O at room temperature. Work-up of the reaction mixture after 18 h, resulted in the isolation of **2** in 15% yield as a dark brown crystalline solid (Scheme 2). The room temperature ^{31}P{^{1}H} NMR spectrum of **2** in benzene-*d*$_6$ features a triplet at 17.1 ppm (J_{PP} =33.8 Hz) and a broad doublet at 10.3 ppm (J_{PP} = 30.4 Hz) in a 1:2 ratio (Figure S12). Importantly, these resonances confirm the presence of **2** in the *in situ* monitoring experiment (Figure 1). The ^{1}H NMR spectrum of **2** in benzene-*d*$_6$ at room temperature features a doublet at 8.08 ppm, which is assignable to *ortho*-CH environment of the Ni-bound phenyl ligand. Also present in this spectrum are resonances at 7.96 (4H) and 7.58 ppm (2H), which are assignable to the *ortho*-CH environments of two

magnetically inequivalent thiophenolate ligands (Figure S11). Finally, the ESI-MS spectrum of **2** in THF, collected in positive mode, features an intense peak at 1065.20 *m/z*, assignable to $[M - Ph + PEt_3]^+$, as well as smaller peaks at 947.10 *m/z* and 988.14 *m/z* , which are ascribable to $[M - Ph]^+$ (calcd 947.01 m/z) and $[M - 2Ph + PEt_3]^+$ (calcd 988.06 m/z), respectively (Figures S27-32). The failure to observe $[M]^+$ in this spectrum is consistent with the expected higher reactivity of an organometallic Ni species.

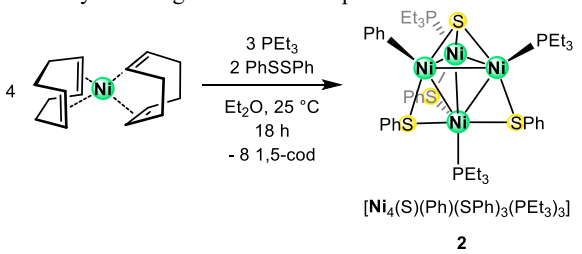

Scheme 2. Synthesis of **2**.

Crystals of **2** suitable for single-crystal X-ray diffraction were grown from a hexanes solution of **2** stored at –25 °C for two months. Compound **2** crystallizes in the triclinic space group *P*-1 as the hexane solvate, **2**·0.5C_6H_{14} (Figure 3). Importantly, the solid-state structure of **2**·0.5C_6H_{14} reveals the presence of the Ni-bound phenyl moiety, as well as a μ_3 sulfide ligand. Evidently, these ligands are derived from a C–S oxidative addition across a low-valent Ni center. Complex **2** features a distorted tetrahedral arrangement of its four Ni atoms. The Ni–Ni distances between Ni1, Ni4, and Ni2 are relatively short (Ni1–Ni4 = 2.5312(8), Ni2–Ni4 = 2.5573(9), Ni1–Ni2 = 2.5641(8) Å; FSR = 1.02, 1.03, and 1.03, respectively), whereas those from Ni1, Ni2, and Ni4 to Ni3 are slightly longer (Ni3–Ni4 = 2.6492(8), Ni2–Ni3 = 2.6853(9), Ni1–Ni3 = 2.7022(7) Å; FSR= 1.06, 1.08, and 1.09, respectively). Finally, the Ni1–C1 distance (1.887(4) Å) is comparable to those found for other low-valent Ni-phenyl complexes.[33-34] Overall, complex **2** features an average oxidation state of +1.5. Its diamagnetism (Figures S11–S12), along with its short Ni–Ni distances, suggest that the Ni valence electrons in **2** are antiferromagnetically coupled and delocalized over all four Ni centers, as was observed for **1**. We next attempted to independently generate complex **3**. Thus, a mixture of 1.5 equiv of PhSSPh, 5 equiv of [Ni(1,5-cod)$_2$], and 4.5 equiv of PEt_3 was heated to 90 °C in toluene for 18 h. Work-up of the reaction mixture and crystallization from MeCN/Et_2O resulted in the deposition of a mixture of $[Ni_5(S)_2(SPh)_2(PEt_3)_5]$ (**3**) and $[Ni_8(S)_5(PEt_3)_7]$ (**4**), as a brown powder (Scheme 3). A $^{31}P\{^1H\}$ NMR spectral analysis of this mixture revealed the presence of **3** and **4** in an approximate 1:2 ratio. Because of their similar solubilities, we could not separate **3** and **4** by selective crystallization, and so we characterized them as a mixture.

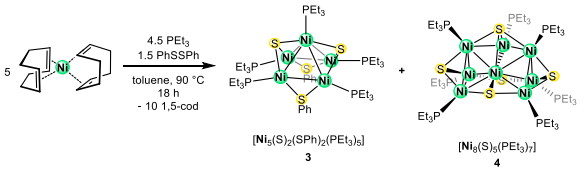

Scheme 3. Synthesis of **3** and **4**.

Crystals of **3** suitable for X-ray crystallography were grown from a concentrated pentane solution of a mixture of **3**, **4**, and **5** left to slowly evaporate at –25 °C for two months. Complex **3** crystalizes in the monoclinic space group $P2_1/c$ (Figure 4). Complex **3** features a square pyramidal arrangement of its five Ni atoms with overall C_s symmetry. Each Ni atom is ligated by one PEt_3 ligand. In addition, **3** possesses two μ_3-sulfide ligands and two μ_2-thiophenolate ligands. One phenyl group exhibits axial stereochemistry, while the other exhibits equatorial stereochemistry. The average Ni–Ni distance from the apical Ni (Ni5) to the square base is 2.65 Å (range = 2.623(8) to 2.663(7) Å), which is consistent with a long Ni–Ni bonding interaction (FSR = 1.07). The Ni–Ni distances within the square base alternate between long and short interactions (e.g., Ni1–Ni2 = 2.786(8), Ni3–Ni4 = 2.789(8), Ni3–Ni1 = 2.994(7), Ni4–Ni2 = 2.983(8) Å), suggesting that a minimal bonding interaction exists between Ni3 and Ni1 and Ni4 and Ni2, respectively. Nonetheless, the diamagnetism of **3**, as evidenced by its $^{31}P\{^1H\}$ NMR spectrum (Figure S22), suggests that the valence d electrons of the five Ni centers are strongly coupled. Finally, complex **3** possesses an average oxidation state of +1.20.

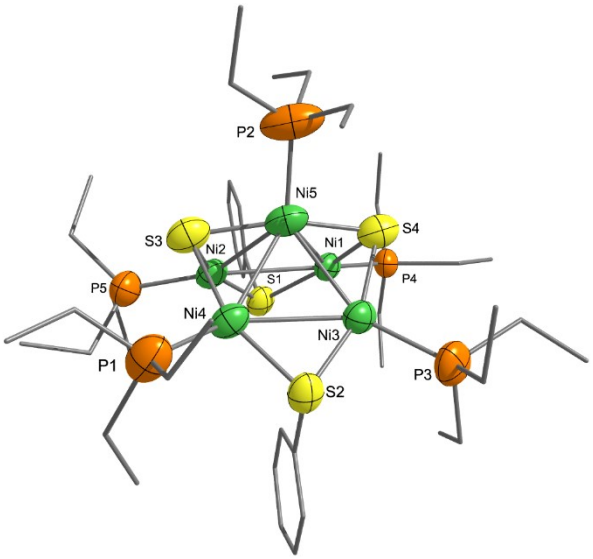

Figure 4. ORTEP diagram of **3** with thermal ellipsoids displayed at 50% probability. Hydrogen atoms are omitted for clarity. Selected distances (Å): Ni5–Ni1 = 2.645(7), Ni5–Ni2 = 2.655(8), Ni5–Ni4 = 2.663(7), Ni5–Ni3 = 2.623(8), Ni1–Ni2 = 2.786(8), Ni3–Ni4 = 2.789(8), Ni3–Ni1 = 2.994(7), Ni4–Ni2 = 2.983(8).

Crystals of **4** suitable for X-ray crystallography were grown from the slow diffusion of acetonitrile into a diethyl ether solution of a mixture **3** and **4** at –25 °C for 7 d. Complex **4** crystallizes in the triclinic space group P-1 (Figure 5). It is isostructural with $[Ni_8(S)_5(PPh_3)_7]$, which was reported by Fenske and co-workers in 1985.[19] Interestingly, $[Ni_8(S)_5(PPh_3)_7]$ was synthesized by reaction of $[NiCl_2(PPh_3)_2]$ and $S(SiMe_3)_2$, followed by reduction with Zn metal, and not by S-atom transfer from PhSSPh. The Ni_8 core of **4** consists of two edge-sharing trigonal bipyramids. Its five sulfide ligands each adopt μ_3 binding modes. In addition, PEt_3 ligands are attached to all but one Ni center. This unique Ni atom (Ni1) appears at the center of the cluster is bonded to the other seven Ni centers with an average Ni–Ni distance of 2.453 Å (range = 2.3871(7) – 2.5223(7) Å). The formal shortness ratios (FRSs) for these distances (0.96 to 1.01) are consistent with those expected for Ni–Ni single bonds.[31, 35] In contrast, the Ni–Ni distances between the peripheral Ni atoms are longer (range = 2.6517(8) Å to 2.8216(8) Å; FSR = 1.07 to 1.13), suggesting weaker metal–metal interactions among these atoms. Similar Ni–Ni distances are observed for $[Ni_8(S)_5(PPh_3)_7]$.[19] Ni1 is also bound to one sulfide ligand (S2) with an Ni–S bond length of 2.1296(9) Å. The unique

coordination environment (and high coordination number) observed for Ni1 is reminiscent of the Ni coordination environments observed for much larger clusters, such as $[Ni_{21}(Se)_{14}(PEt_2Ph)_{12}]$[36] and $[Ni_{23}(Se)_{12}(PEt_3)_{13}]$,[27, 37] suggesting that **4** represents a transition point between small molecular clusters, such as complexes **1**, **2**, and **3**, and much larger NCs.

A $^{31}P\{^1H\}$ NMR spectrum of a mixture of **3** and **4** features a doublet at 4.8 ppm (4P, J_{PP} = 25.6 Hz) and a triplet at 13.4 ppm (1P, J_{PP} = 25.6 Hz), which correspond to the two unique ^{31}P environments expected for complex **3** (Figure S22). Also present in the spectrum are broad singlets at –4.6, 13.1, and 14.9 ppm, which are assignable to complex **4**. These singlets appear in a 4:2:1 ratio. Importantly, these spectral data are identical to those observed in the *in situ* $^{31}P\{^1H\}$ NMR spectrum (Figure 1), confirming their presence in that experiment. The ^1H NMR spectrum of a mixture of **3** and **4** features a series of broad multiplets between 1 and 2 ppm, which are assignable to the PEt_3 ethyl environments of **3** and **4** (Figure S21). This spectrum also features a multiplet at 7.68 ppm, which is assignable to the lone *ortho*-CH phenyl environment of complex **3**. This chemical shift is nearly identical to that observed for **3** in the *in situ* ^1H NMR spectrum (Figures S2–S3), further confirming its presence in that reaction.

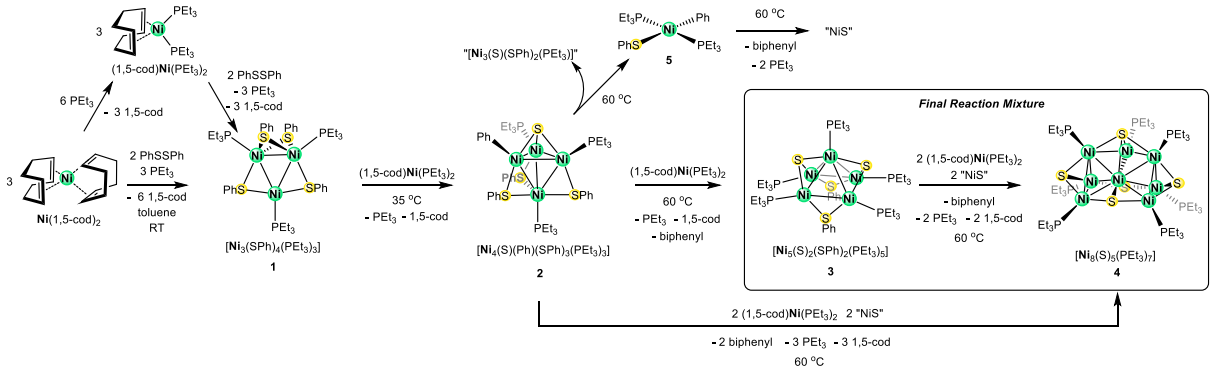

Scheme 4. Proposed reaction sequence that converts $[Ni(1,5\text{-cod})_2]$ into complexes **3** and **4**.

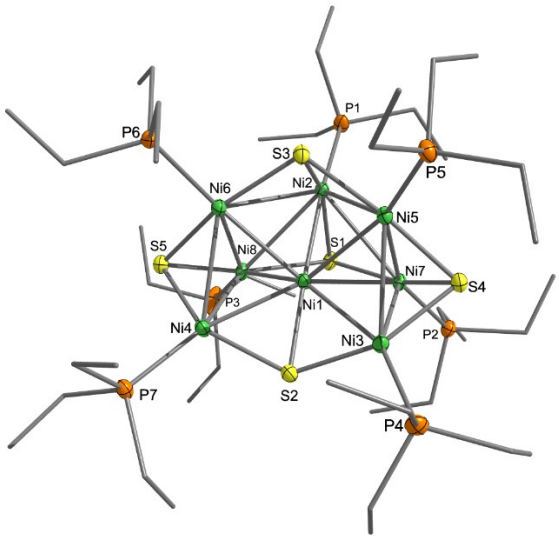

Figure 5. ORTEP diagram of **4** with thermal ellipsoids plotted at 50%. All hydrogen atoms omitted for clarity. Carbon atoms shown as wireframe. Only one set of ethyl groups are displayed for disordered ethyl groups of P3. Selected bond lengths (Å): Ni1–Ni3 = 2.4988(8), Ni1–Ni5 = 2.5223(7), Ni1–Ni6 = 2.4847(6), Ni1–Ni4 = 2.4756(6), Ni1–Ni7 = 2.3982(6), Ni1–Ni8 = 2.4008(8), Ni1–Ni2 = 2.3871(7).

2.3. Mechanistic Considerations

To rationalize our *in situ* $^{31}P\{^1H\}$ and ^1H NMR spectroscopic results, we suggest that the first step involves reaction of $[Ni(1,5\text{-cod})_2]$ with PEt_3 to form $[(1,5\text{-cod})Ni(PEt_3)_2]$ (Scheme 4). This proposed step fits with the reported reactivity of $[Ni(1,5\text{-cod})_2]$, which is known to readily react with monodentate phosphines to form complexes of the type $[(1,5\text{-cod})Ni(PR_3)_2]$.[30, 38-41] We hypothesize that $[(1,5\text{-cod})Ni(PEt_3)_2]$, along with unreacted $[Ni(1,5\text{-cod})_2]$, then react with PhSSPh to form complex **1**, which, according to our $^{31}P\{^1H\}$ and ^1H NMR spectroscopic results, is the major Ni-containing cluster at short reaction times. Its formation can be explained by invoking reaction of PhSSPh with $[(1,5\text{-cod})Ni(PEt_3)_2]$ to form $[Ni(SPh)_2(PEt_3)_2]$ via oxidative addition. 2 equiv of $[Ni(SPh)_2(PEt_3)_2]$ could then couple with either $[Ni(1,5\text{-cod})_2]$ or $[(1,5\text{-cod})Ni(PEt_3)_2]$ to form **1**. It is important to note that all of the PEt_3 and PhSSPh is consumed in the initial stages of the reaction, but not all of the Ni(0) is consumed, which is consistent with the fact that sub-stoichiometric amounts of PEt_3 and PhSSPh were added to the reaction mixture. Significantly, this pool of unreacted Ni(0) (i.e., $[Ni(1,5\text{-cod})_2]$ and $[(1,5\text{-cod})Ni(PEt_3)_2]$) likely plays an important role in cluster growth (see below).

On standing at room temperature, we observe a decrease of **1**, $[Ni(1,5\text{-cod})_2]$, and $[(1,5\text{-cod})Ni(PEt_3)_2]$, and increase in **2**, suggesting that complex **1** converts into **2**, which occurs via formal addition of 1 equiv of "Ni(0)" to **1**, concomitant with a C–S oxidative addition, which converts a thiophenolate ligand into a phenyl ligand and a μ_3-sulfide ligand. The source of "Ni(0)" required to form **2** can be either $[Ni(1,5\text{-cod})_2]$ or $[(1,5\text{-cod})Ni(PEt_3)_2]$, which are abundant at early time scales, according to the $^{31}P\{^1H\}$ and ^1H NMR spectra of the reaction mixture. The amount of complex **3** also slowly increases during the early stages of the reaction. Its formation can be rationalized by invoking addition of an equivalent of "Ni(0)" to **2**, concomitant with a C–S oxidative addition step followed by reductive elimination of biphenyl. This hypothesis is consistent with the observation of biphenyl in the reaction mixture as well as the continued presence of Ni(0) equivalents at this stage of the reaction. We also note that PhSSPh has previously been shown to act as an S-atom donor in the synthesis of Ru sulfide clusters, likely via a similar sequence of oxidative additon and reductive elimination steps.[42]

Upon heating to 40 °C, complex **2** begins to decrease in concentration, while complex **3** continues to increase. Complex **4** also appears in the reaction mixture at this temperature. Its formation can be explained by invoking elimination of biphenyl from **3**, followed by formal addition of 2 equiv of "Ni(0)", 2 equiv of PEt_3, and 1 equiv of "NiS".

Alternatively, complex **4** could be formed directly from **2** via a similar sequence. With prolonged heating, we observe the complete disappearance of **2** and further increases of **3** and **4**, which are the only observable PEt_3-containing clusters at this stage of the reaction. Importantly, this observation is consistent with complex **2** being the precursor to complexes **3** and **4**. While **4** appears to be the ultimate product of the reaction, we suggest that it is just the most stable cluster at these temperatures and time scales. Other, larger clusters can probably be accessed by moving to higher temperatures and longer time scales. Finally, it is important to note that complete conversion of **3** into **4** is likely not observed because of the consumption of all the "Ni(0)" equivalents at later stages of the reaction. It is also interesting to note the apparent absence of Ni_6- and Ni_7-containing clusters, which are probably being generated during the conversion of **3** into **4**. We hypothesize that they are too quickly converted into **4** to be generated in sufficient concentrations to be observed. For comparison, Fenske and co-workers isolated a comparable series of selenide-supported Ni clusters, including $[Ni_4Se_3(P(CH_2CH_2Ph)_3)_5]$, $[Ni_7Se_5(P^iPr_3)_6]$, and $[Ni_8Se_6(PEt_2Ph)_6]$. These clusters were isolated by varying solvent, stoichiometry, and identity of the supporting ligand and were hypothesized to be intermediates to a larger Ni_{21} cluster.[36] While the mechanism of cluster formation is obviously different than in our case, this example is consistent with the step-wise cluster growth that we observe for **3** and **4**.

Consistent with the proposed mechanism of formation of **2** and **3**, reaction of **1** with 1 equiv of $[Ni(1,5\text{-cod})_2]$ results in formation of **2** in 21% yield after 17 h at room temperature, according to the integration of its ^{31}P resonances against an internal standard (Figure S10). Also present in the reaction mixture is a small amount of complex **3**, which formed in 9% yield. To explain the presence of both **2** and **3** in this sample we suggest that the rates of Ni(0) addition to their precursor complexes are similar. Importantly, the observation of both species is evidence for cluster growth by addition of Ni(0) equivalents. The formation of **5** in the reaction mixture is harder to rationalize, as it is the only monometallic species that appears to form during the reaction. Its presence in the reaction mixture was confirmed by X-ray crystallography (Figure S1). It is possible that **5** forms by reaction of PhSSPh with $[(1,5\text{-cod})Ni(PEt_3)_2]$ to form $[Ni(SPh)_2(PEt_3)_2]$, followed by donation of an S-atom to another cluster. Alternatively, its formation can be rationalized by fragmentation of **2** into **5** and the unobserved species, $[Ni_3(S)(SPh)_2(PEt_3)]$, which can serve as a source of atoms and ligands for the growth of other clusters. While the latter route may appear somewhat non-intuitive, it is consistent with the observed reactivity of **2** (Scheme 5). Specifically, heating an independently prepared sample of **2** in benzene-d_6 at 55 °C results in formation of complex **5**, as well as small amounts of **3**, according to the $^{31}P\{^1H\}$ NMR spectrum (Figure S16). Also formed is a small amount of an unidentified PEt_3-containing material. Interestingly, in the *in situ* monitoring experiment (Figure 1e, Table S2) the amount of complex **5** begins to decrease upon prolonged heating, which may be due to its unproductive thermal decomposition. Alternatively, **5** could be serving as the source of "NiS" that is apparently required to form complex **4**. Indeed, the involvement of monometallic complexes in nanocluster growth has come under increased scrutiny in recent years.[43] For example, we demonstrated that the conversion of a Cu_{25} nanocluster into a Cu_{29} nanocluster was mediated by $[(Ph_2phen)(PPh_3)CuCl]$, which acted as a "CuCl" carrier.[44]

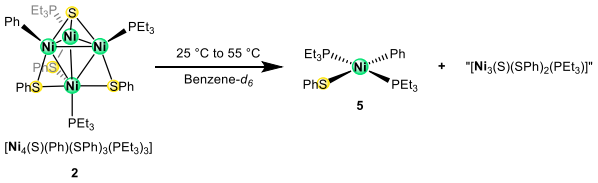

Scheme 5. Thermolysis of **2**.

Several research groups have explored the mechanisms of nanocluster growth over the past decade.[4, 45] These studies have typically employ mass spectrometry to monitor cluster speciation.[46-52] For example, Xie and co-workers have studied the growth of Au_{25} via mass spectrometry. Incredibly, they identify nearly 30 intermediates along the Au_{25} reaction pathway.[11] Likewise, we identified numerous intermediates along the Ni_8 reaction pathway using ^{31}P NMR spectroscopy to monitor cluster growth. While not as widely applicable as mass spectrometry, ^{31}P NMR spectroscopic monitoring is a complementary technique that could find broad utility in nanocluster synthesis, especially given the prevalence of phosphine co-ligands in nanoclusters.

3. Conclusions

In summary, we have shown that reaction of $[Ni(1,5\text{-cod})_2]$ with sub-stoichiometric amounts of the thiolate source, PhSSPh, in the presence of PEt_3, results in initial formation of the low-valent Ni-thiolate cluster, $[Ni_3(SPh)_4(PEt_3)_3]$ (**1**), which then converts into $[Ni_4(S)(Ph)(SPh)_3(PEt_3)_3]$ (**2**), via formal addition of "Ni(0)", along with a C–S oxidative addition step. Complex **2** then converts into a mixture of $[Ni_5(S)_2(SPh)_2(PEt_3)_5]$ (**3**) and $[Ni_8(S)_5(PEt_3)_7]$ (**4**), via further addition of "Ni(0)" equivalents, in combination with a series of C–S oxdiative addition and C–C reductive elimination steps. The isolation of phenyl-containing, organometallic Ni cluster **2** is particularly significant because it clarifies the mechanism by which the sulfide ligand is generated, as well as mechanism by which biphenyl is formed in the reaction mixture. Overall, this work provides an unprecedented level of detail of the early stages of Ni nanocluster growth, and identifies the fundamental reaction steps (i.e., metal(0) atom addition, C–S oxidative addition, and C–C reductive elimination) that are required to grow an individual cluster. In addition, this work uncovers a previously unrecognized route to Ni sulfide NCs, namely, use of PhSSPh as a S-atom source. Finally, and perhaps most importantly, the facile formation of sulfide-containing APNCs from oxidative addition of a bound thiophenolate group demonstrates that the isolation of low-valent, thiolate-stabilized NCs of Ni will be incredibly challenging. Given the proclivity of low-valent Ni to effect C–S oxidative addition, we suggest that thiolate-stabilized NCs of Ni will only be isolable if C–S oxidative addition can be somehow suppressed.

[CCDC 2004575-2004579 contains the supplementary crystallographic data for this paper. These data can be obtained free of charge from The Cambridge Crystallographic Data Centre via www.ccdc.cam.ac.uk/data_request/cif.]

Supporting Information

Supporting Information is available from the Wiley Online Library or from the author.

Acknowledgements

We thank the National Science Foundation (CHE 1764345) for financial support of this work. This research made use of the 400 MHz NMR Spectrometer of the UCSB Chemistry Department, an NIH SIG (1S10OD012077-01A1). The MRL Shared Experimental Facilities are supported by the MRSEC Program of the National Science Foundation under award NSF DMR 1720256; a member of the NSF-funded Materials Research Facilities Network. A. J. T. thanks the Mellichamp Academic Initiative in Sustainability at UCSB for a summer fellowship.

Received: ((will be filled in by the editorial staff))
Revised: ((will be filled in by the editorial staff))
Published online: ((will be filled in by the editorial staff))

References

[1] Q. Yao, T. Chen, X. Yuan, J. Xie, *Acc. Chem. Res.* **2018**, *51*, 1338-1348.

[2] R. W. Huang, J. Yin, C. Dong, A. Ghosh, M. J. Alhilaly, X. Dong, M. N. Hedhili, E. Abou-Hamad, B. Alamer, S. Nematulloev, Y. Han, O. F. Mohammed, O. M. Bakr, *J. Am. Chem. Soc.* **2020**, *142*, 8696-8705.

[3] M. Azubel, R. D. Kornberg, *Nano Lett.* **2016**, *16*, 3348-3351.

[4] R. Jin, C. Zeng, M. Zhou, Y. Chen, *Chem. Rev.* **2016**, *116*, 10346-10413.

[5] I. Chakraborty, T. Pradeep, *Chem. Rev.* **2017**, *117*, 8208-8271.

[6] A. W. Cook, T. W. Hayton, *Acc. Chem. Res.* **2018**, *51*, 2456-2464.

[7] P. D. Jadzinsky, G. Calero, C. J. Ackerson, D. A. Bushnell, R. D. Kornberg, *Science* **2007**, *318*, 430-433.

[8] C. P. Joshi, M. S. Bootharaju, M. J. Alhilaly, O. M. Bakr, *J. Am. Chem. Soc.* **2015**, *137*, 11578-11581.

[9] A. Ghosh, R.-W. Huang, B. Alamer, E. Abou-Hamad, M. N. Hedhili, O. F. Mohammed, O. M. Bakr, *ACS Mater. Lett.* **2019**, *1*, 297-302.

[10] T. Chen, V. Fung, Q. Yao, Z. Luo, D. E. Jiang, J. Xie, *J. Am. Chem. Soc.* **2018**, *140*, 11370-11377.

[11] Z. Luo, V. Nachammai, B. Zhang, N. Yan, D. T. Leong, D. E. Jiang, J. Xie, *J. Am. Chem. Soc.* **2014**, *136*, 10577-10580.

[12] A. W. Cook, G. Wu, T. W. Hayton, *Inorg. Chem.* **2018**, *57*, 8189-8194.

[13] H. N. Kagalwala, E. Gottlieb, G. Li, T. Li, R. Jin, S. Bernhard, *Inorg. Chem.* **2013**, *52*, 9094-9101.

[14] M. Zhu, S. Zhou, C. Yao, L. Liao, Z. Wu, *Nanoscale* **2014**, *6*, 14195-14199.

[15] S. G. Bratsch, *J. Phys. Chem. Ref. Data* **1989**, *18*, 1-21.

[16] A. Gaita-Ariño, F. Luis, S. Hill, E. Coronado, *Nat. Chem.* **2019**, *11*, 301-309.

[17] J. Tejada, E. M. Chudnovsky, E. Del Barco, J. M. Hernandez, T. P. Spiller, *Nanotechnology* **2001**, *12*, 181-186.

[18] A.-H. Lu, E. L. Salabas, F. Schüth, *Angew. Chem. Int. Ed.* **2007**, *46*, 1222-1244.

[19] D. Fenske, J. Hachgenei, J. Ohmer, *Angew. Chem. Int. Ed.* **1985**, *24*, 706-709.

[20] S. Koenig, A. Eichhöfer, N. R. M. Crawford, R. Ahlrichs, D. Fenske, *Z. Anorg. Allg. Chem.* **2007**, *633*, 713-716.

[21] V. W. Day, R. O. Day, J. S. Kristoff, F. J. Hirsekorn, E. L. Muetterties, *J. Am. Chem. Soc.* **1975**, *97*, 2571-2573.

[22] M. G. Thomas, W. R. Pretzer, B. F. Beier, F. J. Hirsekorn, E. L. Muetterties, *J. Am. Chem. Soc.* **1977**, *99*, 743-748.

[23] E. L. Muetterties, E. Band, A. Kokorin, W. R. Pretzer, M. G. Thomas, *Inorg. Chem.* **1980**, *19*, 1552-1560.

[24] A. J. Touchton, G. Wu, T. W. Hayton, *Organometallics* **2020**, *39*, 1360-1365.

[25] E. A. Doud, C. J. Butler, D. W. Paley, X. Roy, *Chem. Eur. J.* **2019**, *25*, 10840-10844.

[26] J. G. Brennan, T. Siegrist, S. M. Stuczynski, M. L. Steigerwald, *J. Am. Chem. Soc.* **1989**, *111*, 9240-9241.

[27] J. G. Brennan, T. Siegrist, Y. U. Kwon, S. M. Stuczynski, M. L. Steigerwald, *J. Am. Chem. Soc.* **1992**, *114*, 10334-10338.
[28] L. R. Narasimhan, T. T. M. Palstra, S. M. Tanzler, M. L. Steigerwald, *Phys. Rev. B: Condens. Matter Mater. Phys.* **1995**, *51*, 9337-9340.
[29] This stoichiometry was chosen because it matches the relative abundance of the components in complex **4**. However, other stoichiometries produce similar results.
[30] L. Cronin, C. L. Higgitt, R. Karch, R. N. Perutz, *Organometallics* **1997**, *16*, 4920-4928.
[31] L. Pauling, *J. Am. Chem. Soc.* **1947**, *69*, 542-553.
[32] R. J. Eisenhart, P. A. Rudd, N. Planas, D. W. Boyce, R. K. Carlson, W. B. Tolman, E. Bill, L. Gagliardi, C. C. Lu, *Inorg. Chem.* **2015**, *54*, 7579-7592.
[33] A. Zeller, E. Herdtweck, T. Strassner, *Eur. J. Inorg. Chem.* **2003**, *2003*, 1802-1806.
[34] H.-F. Klein, A. Bickelhaupt, M. Lemke, H. Sun, A. Brand, T. Jung, C. Röhr, U. Flörke, H.-J. Haupt, *Organometallics* **1997**, *16*, 668-676.
[35] L. Pauling, *Proc. Natl. Acad. Sci. U. S. A.* **1976**, *73*, 4290-4293.
[36] D. Fenske, H. Krautscheid, M. Müller, *Angew. Chem. Int. Ed.* **1992**, *31*, 321-323.
[37] P. Wix, G. E. Kostakis, V. A. Blatov, D. M. Proserpio, S. P. Perlepes, A. K. Powell, *Eur. J. Inorg. Chem.* **2013**, *2013*, 520-526.
[38] Q. Feng, R. Tong, *J. Am. Chem. Soc.* **2017**, *139*, 6177-6182.
[39] H. Maciejewski, A. Sydor, B. Marciniec, M. Kubicki, P. B. Hitchcock, *Inorg. Chem. Acta* **2006**, *359*, 2989-2997.
[40] E. Despagnet-Ayoub, M. K. Takase, J. A. Labinger, J. E. Bercaw, *J. Am. Chem. Soc.* **2015**, *137*, 10500-10503.
[41] H. Schwager, C. Krüger, R. Neidlein, G. Wilke, *Angew. Chem.* **1987**, *99*, 72-73.
[42] N. Begum, M. I. Hyder, M. R. Hassan, S. E. Kabir, D. W. Bennett, D. T. Haworth, T. A. Siddiquee, D. Rokhsana, A. Sharmin, E. Rosenberg, *Organometallics* **2008**, *27*, 1550-1560.
[43] X. Kang, M. Zhu, *Chem. Mater.* **2019**, *31*, 9939-9969.
[44] T.-A. D. Nguyen, Z. R. Jones, D. F. Leto, G. Wu, S. L. Scott, T. W. Hayton, *Chem. Mater.* **2016**, *28*, 8385-8390.
[45] N. Goswami, Q. Yao, T. Chen, J. Xie, *Coord. Chem. Rev.* **2016**, *329*, 1-15.
[46] A. C. Dharmaratne, T. Krick, A. Dass, *J. Am. Chem. Soc.* **2009**, *131*, 13604-13605.
[47] Y. Zhang, Q. Hu, M. C. Paau, S. Xie, P. Gao, W. Chan, M. M. F. Choi, *J. Phys. Chem. C* **2013**, *117*, 18697-18708.
[48] Y. Yu, Z. Luo, Y. Yu, J. Y. Lee, J. Xie, *ACS Nano* **2012**, *6*, 7920-7927.
[49] X. Yang, Y. Su, M. C. Paau, M. M. F. Choi, *Anal. Chem.* **2012**, *84*, 1765-1771.
[50] M. van der Linden, A. J. van Bunningen, M. U. Delgado-Jaime, B. Detlefs, P. Glatzel, A. Longo, F. M. F. de Groot, *J. Phys. Chem. C* **2018**, *122*, 28351-28361.
[51] H. Qian, Y. Zhu, R. Jin, *ACS Nano* **2009**, *3*, 3795-3803.
[52] T. Chen, Q. Yao, R. R. Nasaruddin, J. Xie, *Angew. Chem. Int. Ed.* **2019**, *58*, 11967-11977.

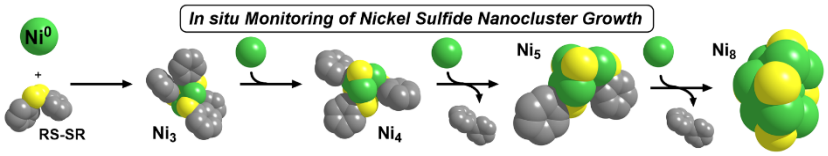

In situ spectroscopic monitoring of nickel sulfide nanocluster formation allows for the identification of the fundamental reaction steps, such as metal atom addition, C–S oxidative addition, and C–C reductive elimination, that occur during cluster growth. This unprecedented level of detail will enable the targeted synthesis of larger Ni sulfide clusters.

Keyword: nickel, thiolate, sulfide, nanocluster, synthesis, mechanism

*Alexander J. Touchton, Guang Wu, Trevor W. Hayton**

Title: Understanding the Early Stages of Nickel Sulfide Nanocluster Growth: Isolation of Ni_3, Ni_4, Ni_5, and Ni_8 Intermediates